Cationic redistribution induced spin-glass and cluster-glass states in spinel ferrite

S. Nayak,[1] S. Ghorai,[2] A. M. Padhan,[3] S. Hajra,[3] P. Svedlindh,[2] and P. Murugavel[1,*]

[1]*Pervoskite Materials Laboratory, Functional Oxides Research Group (FORG), Department of Physics, Indian Institute of Technology Madras, Chennai 600036, India*

[2]*Solid State Physics, Department of Materials Science and Engineering, Uppsala University, Box 35, 75103 Uppsala, Sweden*

[3]*Department of Robotics and Mechatronics Engineering, Daegu Gyeongbuk Institute of Science and Technology (DGIST), Daegu 42988, Republic of Korea*

(Received 17 July 2022; accepted 18 October 2022; published 2 November 2022)

The effect of the cationic redistribution on the complex spinel structure and magnetic properties were investigated in $Zn_{0.7}Cu_{0.3}Fe_2O_4$ ferrite. X-ray photoelectron spectroscopy and x-ray diffraction studies revealed that the system exhibits a mixed spinel structure with Fe^{3+}, Zn^{2+}, and Cu^{2+} occupying both tetrahedral and octahedral sublattices. The DC magnetization results revealed the absence of long-range magnetic order in the system. Furthermore, the AC susceptibility data analysis using dynamic scaling laws suggests that the system exhibits magnetic relaxation below two different temperatures: (i) a spin-glass–like transition at low temperature ($\sim$49.2 K) with critical exponent 10.3 and spin-flip time $\sim 10^{-11}$ s, and (ii) a cluster-glass–like transition at higher temperature ($\sim$317 K) with critical exponent 4.6 and spin-flip time $\sim 10^{-10}$ s. The existence of glassy behavior and magnetic memory effects below the spin-glass transition temperature proves that the system is in nonequilibrium dynamical state. The coexistence of spin-glass and cluster-glass along with the thermal hysteresis between these two transitions could widen the technological applications of these systems.

DOI: 10.1103/PhysRevB.106.174402

I. INTRODUCTION

The effect of disorder on the properties of magnetic materials has been one of the focused areas of research among the magnetism community because of the enthralling physics behind their properties [1]. In disorder-induced spin-glass system, spins are frozen in random directions below a critical temperature [2,3]. Similarly, a cluster-glass is also a magnetically disordered system where blocks of spins are responsible for the slow magnetic relaxation behavior rather than the individual atomic spins [4]. Novel phenomena such as the magnetic memory effect have been discovered in spin-glass and cluster-glass systems below the glass transition temperature [5]. Moreover, the spin-glass theory has unique applications in various areas related to real-world problems. For example, spin-glass models are used to understand neural networks and protein-folding dynamics [6], to design new algorithms for image restoration and machine learning [7], to study the accuracy thresholds of algorithms in quantum computation [8], and to predict the collective price changes of stock portfolios [9]. All these spin-glass models are based on the magnetic disorder and competing magnetic interactions.

The magnetic spinel with a chemical formula AB_2O_4 is known for the interesting physics due to the competing magnetic interactions that arise from their cationic distributions between tetrahedral (A) and octahedral (B) sites [10–14]. Among them, $ZnFe_2O_4$ is one of the important materials due to its exciting magnetic and catalytic properties which make it useful in various technological applications [15–18]. The crystal structure of the normal spinel $[Zn^{2+}]_A[Fe_2^{3+}]_BO_4$ is a close-packed face-centered cubic with Zn^{2+} and Fe^{3+} situated at the A- and B sites, respectively [19–21]. The two Fe^{3+} ions are antiferromagnetically aligned ($\downarrow\uparrow$) at the octahedral sites and thereby make it into an antiferromagnetically ordered system with Néel temperature $T_N \sim 10$ K [22]. Moreover, the cationic redistribution between the A- and B sites plays a significant role in controlling the physical properties of the zinc ferrite [23]. Such cationic redistributions can be induced by ionic substitutions with different radii [24,25]. Singh *et al.* observed that incorporation of Mg^{2+} in $ZnFe_2O_4$ shifts Fe^{3+} from B- to A sites, thereby strengthening the A-B interaction, which has led to large influence on the magnetic properties [26]. Also, Zaki *et al.* reported that Cu^{2+} substitution in place of Zn^{2+} in $Mg_{0.5}Zn_{0.5}Fe_2O_4$ transforms the normal spinel structure into a partially inverted spinel and enhances the saturation magnetization along with the dielectric properties of the material [27]. Reports have shown that Cu^{2+} exhibits high migration rate with low activation energy $E_A \leqslant 0.1$ eV (above 400 °C), which affects the chemical order and site occupancy of the cations in the A and B sublattices [28,29]. Consequently, several exciting magnetic phenomena such as spin-glass behavior, spin-liquid phase, bipolar exchange bias, etc. appeared in the system [30–33]. In this regard, Akhter *et al.* showed that $Cu_{1-x}Zn_xFe_2O_4$ ($x = 0.9$) system exhibits spin-glass behavior when nonmagnetic Zn is substituted in place of Cu [34]. Very recently, the same research group showed that Curie temperature (T_C) shift towards the lower side upon increasing the Zn substitution in $Cu_{1-x}Zn_xFe_2O_4$ ($0 \leqslant x \leqslant 1$) system [35]. They have attributed the decrease in the transition temperature and variation in the magnetic

*muruga@iitm.ac.in

moment to the cationic redistribution between *A*- and *B* sites [34,35]. However, a detailed study on the low-temperature magnetic behavior of such cationic disordered spinel ferrite systems is still lacking.

This work is mainly focused on the magnetic behavior of the $Zn_{0.7}Cu_{0.3}Fe_2O_4$ in an attempt to address the nature of the magnetic ordering down to low temperature. Structural and electronic properties show that the sample belongs to a partially inverted or mixed spinel family. The frequency-dependent AC susceptibility results show the existence of cluster-glass and spin-glass transitions at 317.1 and 49.2 K, respectively, in the same system which is a unique characteristic observed in any magnetic spinel. Notably, the system exhibits a thermal hysteresis over a wide temperature range between the spin-glass and cluster-glass transitions. Detailed methodology, experimental results, and the analysis, along with their discussions, are presented in this work.

II. EXPERIMENT DETAILS

The solid-state reaction method was employed to synthesize polycrystalline $Zn_{0.7}Cu_{0.3}Fe_2O_4$ using ZnO (Alfa Aesar, purity 99.9%), Fe_2O_3 (Alfa Aesar, purity 99.9%), and CuO (Alfa Aesar, purity 99.9%) as precursors. The stoichiometric mixture of the precursors was ground in an agate mortar for 3 h to homogenize the mixture. The ground powder was calcined at 600 °C for 4 h in a box furnace. After mixing the powder with polyvinyl alcohol as a binder, the calcined powder was pressed into a 12-mm-diameter pellet under ∼14−MPa uniaxial pressures. Finally, the pellet was sintered at 775 °C for 4 h.

The crystal structure and phase purity of the compound were examined by performing x-ray diffraction (XRD) measurements using a Rigaku-make x-ray diffractometer (model: Super MiniFlex 6G) with Cu−K_α radiation ($\lambda = 1.5406$ Å). The microstructure of the sample was investigated by field-emission scanning electron microscopy (FESEM) (model: Quanta 3D FEG). The electronic properties and the chemical compositions of the materials were investigated by x-ray photoelectron spectrometer (XPS) (model: Thermo Fisher, Escalab 250 Xi) with a monochromatic Al − K_α (1486.6-eV) x-ray source at a base pressure of 10^{-7} mbar. The XPS instrument was operated in the constant analysis energy mode after the calibration using the graphitic C-1*s* line at 284.5 eV. Both the DC and frequency-dependent AC magnetic susceptibility measurements along with magnetic memory measurements were performed in a Quantum Design Magnetic Property Measurement System XL in the temperature range 5–380 K. The temperature-dependent heat-capacity data $C_P(T)$ were recorded using a Quantum Design Physical Property Measurement System.

III. RESULTS AND DISCUSSION

A. X-ray photoelectron spectroscopy

To confirm the composition and the cationic site occupancy of the synthesized spinel compound, XPS spectra were recorded on the sample and the results are displayed in Figs. 1(a)–1(d). Figure 1(a) shows the XPS spectrum of the Zn-2*p* core level which exhibits two sharp peaks centered at

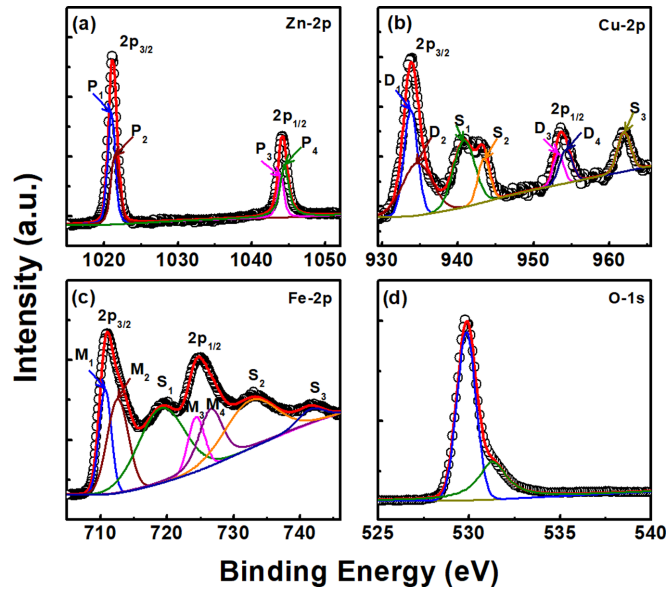

FIG. 1. (a) Core-level XPS spectra of (a) Zn-2*p*, (b) Cu-2*p*, (c) Fe-2*p*, and (d) O-1*s*.

1021.1 eV ($2p_{3/2}$) and 1044.2 eV ($2p_{1/2}$) without any signature of satellite peaks. The difference in binding energy between $2p_{3/2}$ and $2p_{1/2}$, $\Delta E_{2p3/2-2p1/2} \sim 23.1$ eV confirms the existence of Zn^{2+} in the system [36]. Generally, Zn^{2+} prefers to occupy the tetrahedral sites of the lattice, but due to the cationic redistribution they can also migrate and occupy the octahedral sites [37,38]. In the present study, the XPS spectra were fitted using Gaussian-Lorentzian peak functions, which show that the Zn-$2p_{3/2}$ and Zn-$2p_{1/2}$ peaks can be further deconvoluted into two peaks each. The deconvoluted Zn-$2p_{3/2}$ peaks are labeled as P_1 (1021.0 eV) and P_2 (1021.5 eV), whereas the deconvoluted Zn-$2p_{1/2}$ peaks are labeled as P_3 (1043.9 eV) and P_4 (1044.4 eV). The P_1 and P_3 peaks can be ascribed to the presence of Zn^{2+} in the tetrahedral sites, whereas the P_2 and P_4 peaks can be ascribed to the presence of Zn^{2+} in the octahedral sites [37–39]. Figure 1(b) represents the Cu-2*p* core-level XPS spectra, which show two major peaks, Cu-$2p_{3/2} \sim 934$ eV and Cu-$2p_{1/2} \sim$ 953.6 eV, along with three satellite peaks located at 940.7, 943.1, and 962 eV, respectively. The difference in binding energies $\Delta E_{2p3/2-2p1/2} \sim 19.6$ eV confirms the existence of the divalent oxidation state of Cu [40]. The XPS fitting analysis depicts that the Cu-$2p_{3/2}$ peak can be further deconvoluted into two peaks located at 933.8 eV (D_1) and 934.7 eV (D_2). Moreover, the Cu-$2p_{1/2}$ peak can also be deconvoluted into two peaks centered at 953.3 eV (D_3) and 954.3 eV (D_4). The D_2 and D_4 peaks of Cu-$2p_{3/2}$ and Cu-$2p_{1/2}$ are assigned to the presence of Cu^{2+} in tetrahedral sites of the lattice, whereas the D_1 and D_3 peaks are assigned to the presence of Cu^{2+} in octahedral sites of the spinel [41].

Figure 1(c) shows the XPS spectra of the Fe-2*p* core level, which exhibit two characteristic peaks at 711.1 and 724.8 eV corresponding to Fe-$2p_{3/2}$ and Fe-$2p_{1/2}$, respectively, along with three satellite peaks labeled as S_1 (719.4 eV), S_2 (733 eV), and S_3 (743.1 eV). The two major Fe-2*p* peaks are further deconvoluted into two peaks each. The peaks

TABLE I. Cationic distribution in the octahedral and tetrahedral sites of $Zn_{0.7}Cu_{0.3}Fe_2O_4$ obtained from XPS analysis.

Atoms	*A* sites (%)	*B* sites (%)
Zn	53	47
Cu	37	63
Fe	26	74

positioned at ∼710.9 eV (M_1) and ∼724.5 eV (M_3) are related to the presence of Fe^{3+} at the *B*-site sublattice, and the peaks located at ∼713.2 eV (M_2) and ∼726.8 eV (M_4) are related to the presence of Fe^{3+} at the *A* site of the spinel compound [40,42]. The isomer shifts obtained from the Mössbauer spectroscopy confirm that only the trivalent state of Fe ion is present in the presently studied system (described in Supplemental Material [43]). The O-1*s* spectrum is deconvoluted into two peaks centered at 529.9 and 531.3 eV, which signify the presence of lattice oxygen as well as surface oxygen in this compound [shown in Fig. 1(d)] [44,45]. The percentage occupancy of the Cu^{2+}, Zn^{2+}, and Fe^{3+} cations in tetrahedral and octahedral sites estimated from the area under the respective XPS spectral peaks is displayed in Table I. Table I confirms that the synthesized compound is crystallized in a mixed spinel structure with the chemical formula $(Zn_{0.37}Cu_{0.11}Fe_{0.52})_A[Fe_{1.48}Zn_{0.33}Cu_{0.19}]_BO_4$.

B. X-ray diffraction

The XRD pattern recorded in $\theta-2\theta$ geometry is displayed in Fig. 2(a). The pattern indicates that the compound has formed without any secondary phases. To extract the structural details, the XRD data were subjected to Rietveld refinement using the FULLPROF software. Note that parameters such as site occupancy in the octahedral and tetrahedral sites obtained from the XPS analysis were used as initial parameters during the refinement. The peaks were fitted using a pseudo-Voigt profile and a Chebychev polynomial was used to refine the background profile. The refinement shows that $(Zn_{0.37}Cu_{0.11}Fe_{0.52})_A[Fe_{1.48}Zn_{0.33}Cu_{0.19}]_BO_4$ belongs to the cubic spinel family with Fd-3m (227) space group. The extracted structural parameters, *viz*., lattice constants, interaxial angles, isothermal parameter, and positional coordinates, are listed in Table II. The better values of the goodness of the fit (χ^2) and residual weight percent (R_{wp}) of the Rietveld refinement reconfirms the conclusion drawn from XPS analysis. The corresponding crystal structure generated from VESTA software is displayed in Fig. 2(b). The calculated bond lengths ($A-O = 1.92$ Å and $B-O = 2.06$ Å) and bond angles ($< A-O-B = 123.06^\circ$ and $< B-O-B = 93.06^\circ$) of the spinel compound are shown in Fig. 2(b). It is observed that both $< A-O-B$ and $< B-O-B$ bond angles are tilted by ∼3° from their undistorted values. Such tilting can also influence the magnetic ordering of the sample. The FESEM recorded for the morphology of the sample is shown in Fig. 2(c) and it indicates the presence of a uniform distribution of irregular polyhedral-shaped grains in the sample. The histogram analysis and log-normal curve fitting displayed in the inset of Fig. 2(c) reveals that the average grain size of the material is ∼163 nm.

C. Susceptibility

The temperature-dependent DC magnetic susceptibility $[\chi_{DC}(T) = M/H_{DC}]$ recorded in zero-field-cooled (ZFC) and field-cooled (FC) conditions in the temperature range $5\text{ K} \leqslant T \leqslant 380$ K under the magnetic field of 10 mT are shown in Fig. 3. Interestingly, χ_{DC} does not reveal any feature signaling a transition to long-range magnetic ordering, but a bifurcation between $\chi_{ZFC}(T)$ and $\chi_{FC}(T)$ is observed at about 195 K, denoted as T_{br}. The upturn of χ_{FC} at low temperature can be due to a magnetocrystalline effect [46]. The lack of long-range magnetic ordering and the associated cationic disorder in the system could lead to interesting magnetic states like relaxor or glassy behavior.

There are several experimental techniques used to investigate the slow magnetic relaxation of magnetically disordered systems. Among them, frequency-dependent AC magnetic measurements give evidence of the glassy behavior. Therefore, we studied the temperature-dependent AC magnetic susceptibility at various frequencies, $0.51\text{ Hz} \leqslant f \leqslant 170$ Hz under an AC magnetic field (H_{DC}) of 0.4 mT. Figures 4(a) and

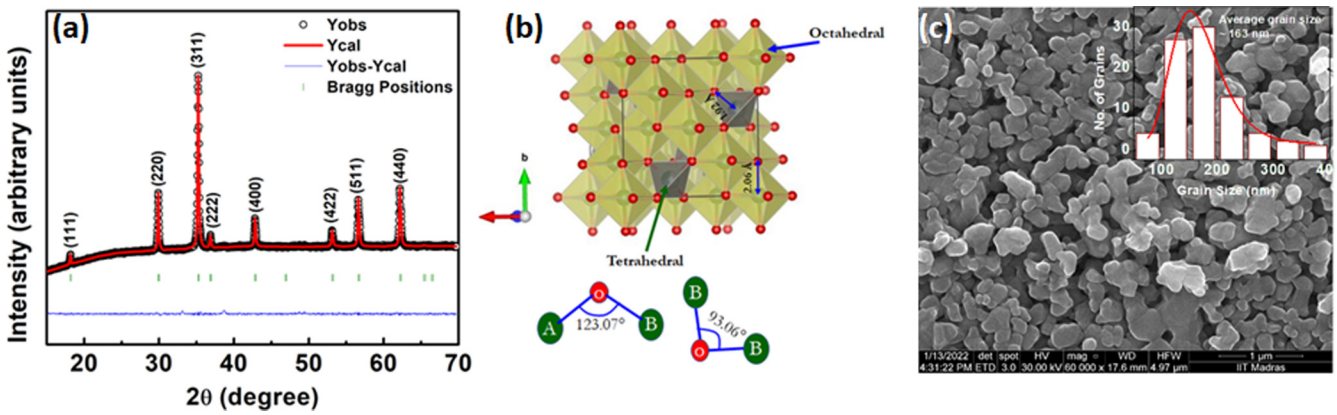

FIG. 2. (a) XRD pattern along with the corresponding Rietveld refinement model of $Zn_{0.7}Cu_{0.3}Fe_2O_4$. (b) The crystal structure of the $Zn_{0.7}Cu_{0.3}Fe_2O_4$ system obtained from VESTA software. (c) FESEM micrograph of $Zn_{0.7}Cu_{0.3}Fe_2O_4$. Inset shows the histogram analysis to calculate average particle size. The solid red line shows the best fit using Log-Normal function.

TABLE II. Structural parameters obtained from the Rietveld refinement analysis. Here, a, b, c, α, β, and γ are the respective structural parameters. R_{wp}, χ^2, U_{iso}, and Occ are the residual weight percent, goodness of the fit, thermal parameter, and the site occupancies, respectively.

	$a = b = c = 8.4392(2) \pm 0.0012$ Å $\alpha = \beta = \gamma = 90^\circ$			$R_{wp} \sim 6.77$; $\chi^2 = 2.62$	
Atoms	x	y	z	U_{iso} (Å^2)	Occ.
Fe1	0.0	0.0	0.0	0.002 83(6)	0.74
Zn1	0.0	0.0	0.0	0.002 83(6)	0.165
Cu1	0.0	0.0	0.0	0.002 83(6)	0.095
O	0.244 08(3)	0.244 08(3)	0.244 08(3)	0.013 19(6)	1
Zn2	0.375	0.375	0.375	0.009 34(6)	0.37
Cu2	0.375	0.375	0.375	0.009 34(6)	0.11
Fe2	0.375	0.375	0.375	0.009 34(6)	0.52

4(b) show the temperature-dependent in-phase $[\chi'(T)]$ and out-of-phase $[\chi''(T)]$ components of the AC susceptibility $[\chi_{AC}(T) = M(T)/H_{AC}]$ in the temperature range 5–380 K, respectively. For clarity, the enlarged version of the plots over a small temperature range is shown as an inset in the respective plots. From the insets of Fig. 4(a), clear frequency dispersion is observed, which signifies the existence of glassy behavior in this system [33]. Interestingly, the out-of-phase component shown in Fig. 4(b) exhibits two peaks ($\sim$ 40 and 290 K), indicating the existence of two separate glassy behaviors.

The Mydosh parameter (S) can be used to understand the relative shift of χ_{AC} with frequency as seen in Fig. 4(b). The expression of the Mydosh parameter $S = \Delta T_f/(T_f\ \Delta\ \log_{10} f)$, where $\Delta T_f = T_f(f_1) - T_f(f_2)$ and $\Delta\ \log_{10} f = \log_{10} f_1 - \log_{10} f_2$, f_1 and f_2 are the initial and final frequencies. T_f indicates the freezing temperature corresponding to the high-temperature side of the full width at half maxima point in the $\chi''(T)$ plot shown in Fig. 4(b). Here, we have chosen f_1 and f_2 as 0.51 and 170 Hz, respectively. Accordingly, the values of S obtained from the above analysis are 0.03 (low-temperature glassy behavior around 40 K) and 0.009 (high-temperature glassy behavior around 290 K), respectively. For a spin-glass system, the expected value S should be within 0.005–0.08, and for a superparamagnetic behavior $S > 0.2$ [2]. In the present case, the calculated values of S are within the range for a spin-glass system.

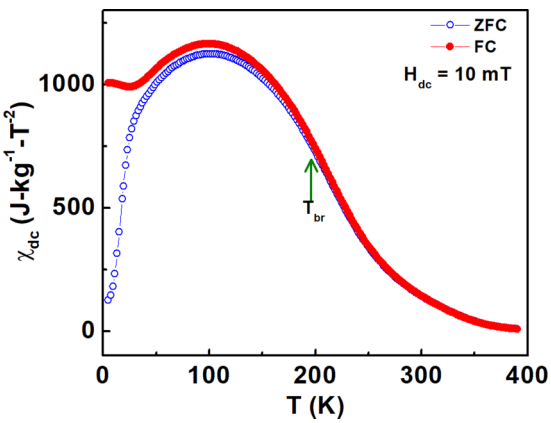

FIG. 3. Temperature-dependent DC magnetic susceptibility $\chi_{DC}(T)$ for $Zn_{0.7}Cu_{0.3}Fe_2O_4$ measured under ZFC and FC conditions.

To explore further about the spin-glass or cluster-glass behavior of the $Zn_{0.7}Cu_{0.3}Fe_2O_4$ spinel ferrite, we used two dynamical scaling laws: (i) the power-law scaling and (ii) the Vogel-Fulcher law. The power-law scaling describes the critical slowing down of the magnetic relaxation and can be expressed as $\tau = \tau_0\ (T/T_g - 1)^{-z\nu}$, where $\tau = 1/2\pi f$ describes relaxation time corresponding to the probing frequency f, T_g is spin-glass transition temperature, τ_0 is related to the single spin-flip time, z is the dynamical critical constant, and ν represents the critical exponent of the correlation length $\zeta = (T/T_g - 1)^{-\nu}$. According to the dynamical scale hypothesis, τ is related to ζ as $\tau \sim \zeta^z$. Using the definition of the frequency-dependent freezing temperature as mentioned above, we plot the logarithmic variation of relaxation time as a function of the logarithm of $[(T - T_g)/T_g]$ for the low-temperature transition ($\sim$40 K) in Fig. 5(a). The solid red lines show the best fitting obtained using power-law scaling. The fitting yields the value of $T_g = 49.2$ K, $\tau_0 = 7.3 \times 10^{-11}$ s, and critical exponent $z\nu = 10.3$. For a conventional spin-glass system, $z\nu$ should lie between 4 and 12, and τ_0 should lie between 10^{-10} and 10^{-13} s, while for a cluster-glass system, τ_0 should lie between 10^{-7} and 10^{-10} s [2,47,48]. By comparison to the parameters obtained from the power-law scaling analysis, it is confirmed that the dispersion seen in the low-temperature susceptibility data is associated with the presence of spin-glass phase with $T_g = 49.2$ K.

On the other hand, the empirical Vogel-Fulcher law for interacting particle systems can be expressed as $\tau = \tau_0 \exp[E_a/k_B(T - T_0)]$, where T_0 is a measure of the magnetic interaction and E_a is activation energy. Accordingly, the logarithmic variation of τ plotted as a function of $1/(T - T_0)$ is shown in Fig. 5(b). The best fit obtained from the Vogel-Fulcher analysis yields $T_0 = 42.2$ K and $\tau_0 = 7.1 \times 10^{-11}$ s. Again, the value of τ_0 suggests a spin-glass behavior exists in the system [49]. According to de Strooper *et al.*, the random cationic distribution (magnetic and nonmagnetic elements) leads to competing exchange interactions between magnetic moments in the A- and B sites of spinel system [50]. Such competing interactions create magnetic frustration which may lead to the formation of spin clusters in the system [49–51]. However, the low-temperature dynamics observed in the present system depicts the characteristic of a spin-glass behavior. To understand the nature of the magnetic relaxation

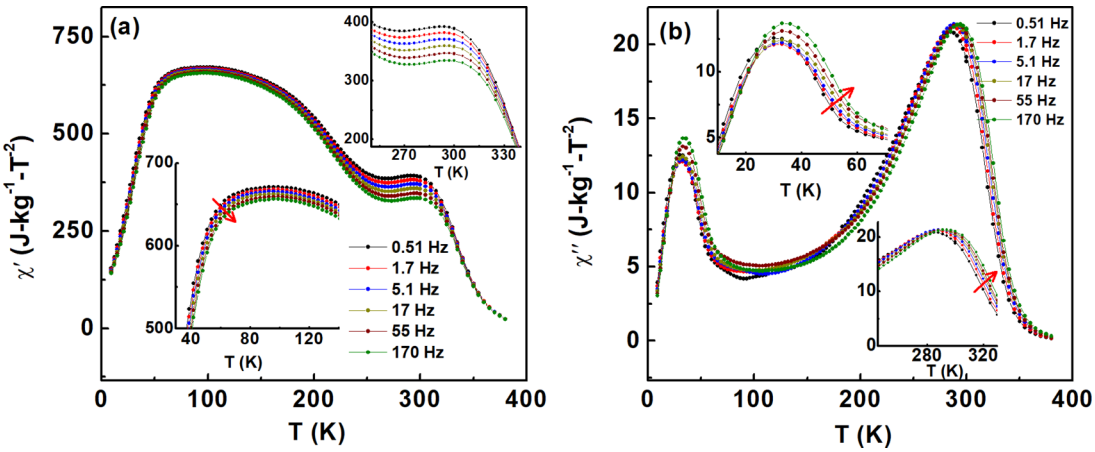

FIG. 4. Temperature-dependent AC magnetic susceptibility: (a) real part (χ') and (b) imaginary part (χ'') of $Zn_{0.7}Cu_{0.3}Fe_2O_4$ measured at 0.51 Hz $\leqslant f \leqslant$ 170 Hz. Top and bottom insets of (a) show the enlarged portions around 310 and 59 K, respectively. Top and bottom insets of (b) show the enlarged portions around 40 and 290 K, respectively.

observed around 290 K, we have used the dynamic scaling laws (power-law scaling and Vogel-Fulcher law). Figure 5(c) shows the resultant data fitted with power-law scaling which yields the value of $T_g = 317.1$ K, $\tau_0 = 3.1 \times 10^{-10}$ s, and the critical exponent $z\nu = 4.6$. These observed values signify the presence of cluster glass in the system. An equally good fit is obtained from the Vogel-Fulcher analysis with $T_0 = 304.3$ K and $\tau_0 = 5.9 \times 10^{-9}$ s, again indicating the presence of interacting spin clusters in this system [as shown in Fig. 5(d)]. Overall, the AC susceptibility analysis reveals that the system exhibits spin-glass behavior at low temperature,

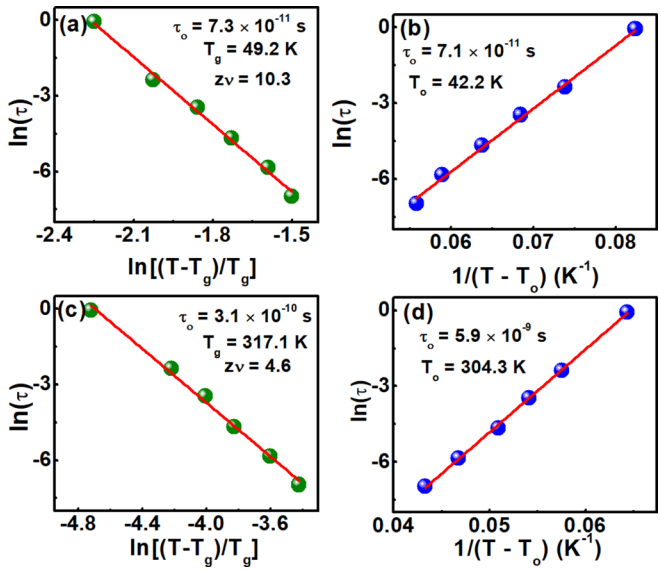

FIG. 5. (a) The best fit (solid red line) to the logarithmic variation of relaxation time using power-law scaling around 40 K. (b) Logarithmic variation of relaxation time as a function of $1/(T–T_o)$. The solid red line shows the best fit using Vogel-Fulcher law (around 40 K). (c) The best fit (solid red line) to the logarithmic variation of relaxation time using power-law scaling around 290 K. (d) Logarithmic variation of relaxation time as a function of $1/(T–T_o)$. The solid red line shows the best fit using Vogel-Fulcher law (around 290 K).

~49.2 K, where the magnetic spins freeze in random directions and cluster-glass behavior at high temperature around 317.1 K, where the magnetic spins form clusters.

D. Magnetic memory effect

In order to explore the low-temperature spin-glass dynamics, magnetic memory effect measurements were carried out in the presence of DC and AC applied magnetic field conditions separately under stop and wait protocols. Figure 6(a) shows the temperature-dependent FC susceptibility data measured under this protocol at DC applied magnetic field $H_{DC} =$ 2 mT. In this protocol, the sample was cooled down from 390 to 5 K at a cooling rate of 1 K/min under H_{DC}. After that, the sample was warmed up to 390 K while recording the temperature-dependent DC susceptibility [denoted as χ^{ref}_{FCW} in Fig. 6(a)] in the presence of H_{DC}. In the next step, the sample was cooled down to 5 K while recording the DC susceptibility. During this measurement, the cooling process was interrupted by a 2-h halt at 290 and 40 K, respectively, and the H_{DC} was switched off during the halt period. The measured FC susceptibility under this process is denoted as χ^{stop}_{FCC} in Fig. 6(a). Again, the sample was heated up to 350 K while recording the DC susceptibility without any interruption. The data obtained during this warming cycle are designated as χ^{mem}_{FCW} in Fig. 6(a). We observed a noticeable steplike behavior at 40 K [inset of Fig. 6(a)], whereas the sharp steplike behavior is absent at 290 K. It is observed from the figure that the χ^{mem}_{FCW} data (red color) follows the χ^{stop}_{FCC} curve (green color) below the stopping temperature (40 K), but it makes a jump, bringing its value close to χ^{ref}_{FCW} (blue color) at the stopping temperature. The observed feature clearly signifies the presence of magnetic memory in the system.

Secondly, in the ZFC-susceptibility protocol, the sample was cooled down from 350to 5 K with a 2-h halt each at 290 and 40 K. After reaching 5 K, $H_{DC} = 2$ mT was applied and the magnetization was measured with increasing temperature, which is denoted as χ^{mem}_{ZFC} in Fig. 6(b). Here, we also recorded a reference curve by following the usual ZFC protocol in an applied field of 2 mT [denoted as χ^{ref}_{ZFC} in Fig. 6(b)]. From the

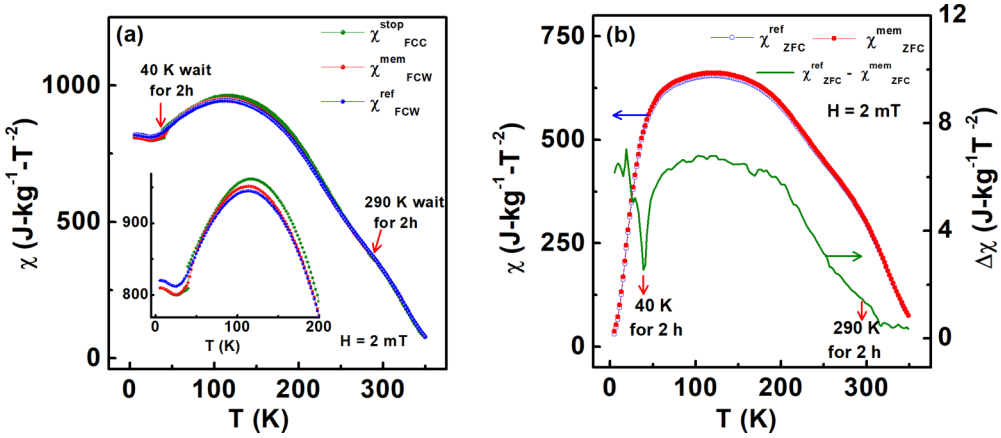

FIG. 6. Measurements of memory effect as a function of temperature in (a) FC and (b) ZFC protocols with $H_{DC} = 2$ mT. Inset (a) shows the zoomed view around 40 K where the measurement was interrupted for 2 h (as discussed in the text).

figure, we noticed that both χ^{mem}_{ZFC} and χ^{ref}_{ZFC} almost coincide with each other apart from the stopping-temperature region. The right-hand side of Fig. 6(b) represents the difference in susceptibility $\Delta\chi = \chi^{ref}_{ZFC} - \chi^{mem}_{ZFC}$ as a function of temperature. Note that the $\Delta\chi$ curve clearly shows a dip at the stopping temperature 40 K, whereas such feature is absent at 290 K. The presence of memory dip at 40 K is a signature of the spin-glass state, while its absence at 290 K suggests different glassy dynamics.

From the temperature-dependence of the FC susceptibility we noticed a thermal hysteresis behavior between warming and cooling curves, i.e., between χ^{ref}_{FCW} and χ^{stop}_{FCC} in Fig. 6(a). To probe it further, we measured the FC susceptibility as a function of temperature during both warming and cooling cycles. The procedure is as follows: (i) First, the sample was cooled to 5 K in absence of H_{DC} and then the ZFC susceptibility was recorded while warming under $H_{DC} = 0.5$ mT. (ii) After reaching 375 K, the sample was again cooled to 5 K in the presence of the same field and the field-cooled cooling (FCC) susceptibility was recorded. (iii) At the end, the field-cooled-warming (FCW) susceptibility was recorded while the sample was heated up to 375 K in the same magnetic field. The corresponding magnetization versus temperature curves are displayed in Fig. 7. Interestingly, the figure shows irreversibility in susceptibility data between FCC and FCW curves, i.e., a thermal hysteresis is observed over a wide temperature range 50 K $< T <$ 280 K (shown in the inset of Fig. 7). According to Musicó *et al.*, the irreversibility indicates the existence of a spin-glass state in the system due to the slow spin dynamics. Consequently, the system is out of equilibrium at all temperatures below the spin-glass temperature while attempting to reach lower energy state [52]. In the present case, the irreversibility is most apparent in the cluster-glass state.

Furthermore, a memory effect measurement was also carried out using the AC magnetic susceptibility under a stop and wait protocol. Figure 8 shows the temperature-dependent out-of-phase susceptibility results (at 4 Oe and 0.51 Hz) obtained from the magnetic memory measurements. Firstly, the sample was cooled from 351 to 9 K under the AC field with a stop for ∼1.5 h at 300 and 24 K each. The AC magnetic susceptibility recorded during this process is denoted as $\chi''^{stop}_{cooling}$. Secondly, after reaching 9 K, the sample was heated to 351 K without any interruption in the heating process; the AC magnetic susceptibility recorded during this process is denoted as $\chi''^{ref}_{heating}$. It is interesting to note that the sample at both stop temperatures (see the insets in Fig. 8) exhibits a logarithmically slow relaxation, i.e., the sample is in a nonequilibrium state at constant temperature while relaxing towards lower energy state. This is in accordance with the expectations for glassy spin dynamics driven by disordered and frustrated magnetic interactions. The observed relaxation behavior (insets in Fig. 8) near the spin-glass state (24 K) is much stronger than the relaxation near the cluster-glass state (300 K). The right-hand scale of Fig. 8 shows the difference in susceptibility $\Delta\chi'' = \chi''^{ref}_{heating} - \chi''^{stop}_{cooling}$ as a function of temperature. Here, we observe a prominent memory dip at 24 K, while the observation at 300 K is a feature extending over a comparably broad temperature range. Again, the memory dip observed at 24 K is in accordance with expectations of a spin glass, while the broad feature seen around

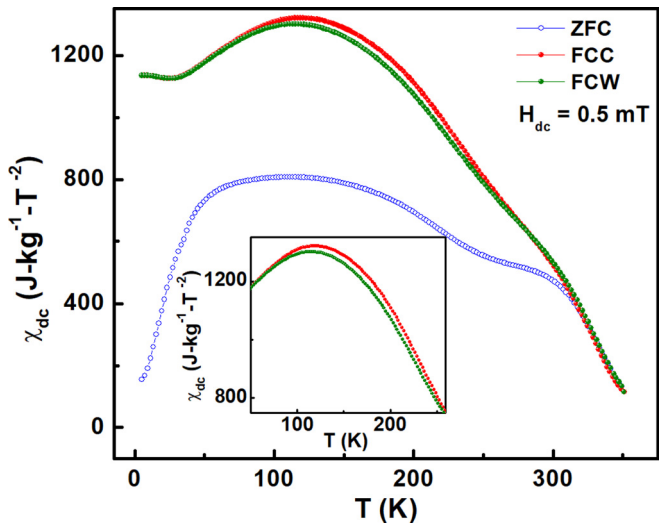

FIG. 7. Temperature-dependent DC susceptibility measured under ZFC, FCC, and FCW modes. Inset shows the zoomed view of FCC and FCW in the temperature range 50 K $< T <$ 280 K.

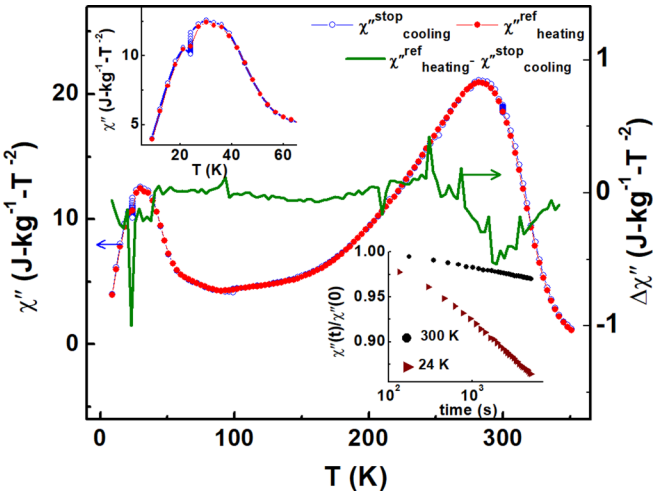

FIG. 8. Measurements of out-of phase susceptibility (χ'') as a function of temperature under stop and wait protocols at 300 and 24 K for ∼1.5 h to study the memory effect. Inset (top) shows zoomed view around 24 K (as discussed in the text). Inset (bottom) shows the imaginary part of AC susceptibility normalized with its value at relative zero time $[\chi''(t)/\chi''(0)]$ as a function of relative time.

300 K does not concur with expectations of a spin-glass. Instead, it is identified as a footprint of the cluster-glass state.

IV. CONCLUSIONS

In summary, the incorporation of Cu^{2+} in Zn sites modifies the crystal chemistry and cationic distribution of the $Zn_{0.7}Cu_{0.3}Fe_2O_4$ spinel. Consequently, the normal spinel $[Zn^{2+}]_A[Fe^{3+}]_BO_4$ transforms to a partially inverted or mixed spinel. XPS results confirm that 26% of Fe^{3+} migrates from octahedral sites to tetrahedral sites, while 47% Zn^{2+} and 63% Cu^{2+} sits on the octahedral sites. Rietveld refinement on the XRD data further confirms that the system belongs to mixed spinel family with cubic crystal structure. The geometric frustration induced by the cationic redistribution disrupts the long-range ordering of the systems and develops spin-glass and cluster-glass states. The AC magnetic susceptibility analysis reveals that the system exhibits two distinctly different relaxation behaviors: (i) below ∼49.2 K and (ii) below ∼317 K. Furthermore, the power-law and Vogel-Fulcher analysis of the AC susceptibility data confirm that the transition at 49.2 and 317 K corresponds to the spin-glass and cluster-glass transitions, respectively. The observed spin-glass behavior of the system at low temperature is reconfirmed by the presence of the magnetic memory effect. It is noteworthy to mention that the temperature-dependent DC susceptibility measurements display a thermal hysteresis behavior due to the random frozen spins over a broad temperature range between cluster-glass and spin-glass transition temperatures. Overall, the results demonstrate that the creation of magnetic disorder via cationic redistribution leads to the formation of spin-glass and cluster-glass in the same system, which is rarely observed in spinel systems.

ACKNOWLEDGMENTS

S.N. acknowledges Science and Engineering Research Board for partial support under the National Postdoctoral fellowship program at Indian Institute of Technology Madras (Project No. SP20210936PHSERB008268, File No. PDF/2020/001921). P.M. acknowledges the Centre of Excellence program through Institute of Eminence (IoE) initiative scheme by the IIT Madras for the financial and logistical support to FORG. S.G. and P.S. gratefully acknowledge the Swedish Foundation for Strategic Research (SSF, Contract No. EM-16-0039) and Infrastructural grants by VR-RFI (Grant No. 2017–00646_9). This work was partially carried out using the facilities of UGC-DAE CSR, Indore. S.N. and P.M. acknowledge Dr. V. R. Reddy UGC-DAE CSR, Indore, for helping in Mössbauer characterization.

[1] N. Rajeesh Kumar, R. Karthik, L. Vasylechko, and R. Kalai Selvan, J. Phys.: Condens. Matter **32**, 245802 (2020).
[2] J. A. Mydosh, *Spin Glasses: An Experimental Introduction* (Taylor & Francis, London, 1993).
[3] J. A. Mydosh, J. Magn. Magn. Mater. **157-158**, 606 (1996).
[4] V. K. Anand, D. T. Adroja, and A. D. Hillier, Phys. Rev. B **85**, 014418 (2012).
[5] K. Jonason, E. Vincent, J. Hammann, J. P. Bouchaud, and P. Nordblad, Phys. Rev. Lett. **81**, 3243 (1998).
[6] G. Parisi, Proc. Natl. Acad. Sci. USA **103**, 7948 (2006).
[7] A. Ansari, J. Berendzen, S. F. Bowne, H. Frauenfelder, I. E. Iben, T. B. Sauke, E. Shyamsunder, and R. D. Young, Proc. Natl. Acad. Sci. USA **82**, 5000 (1985).
[8] J. Inoue, Phys. Rev. E **63**, 046114 (2001).
[9] A. Hirose, S. Ozawa, K. Doya, K. Ikeda, M. Lee, and D. Liu, Eds., *Neural Information Processing - ICONIP 2016* (Springer, Cham, 2016), pp. 579–586.
[10] W. Schiessl, W. Potzel, H. Karzel, M. Steiner, G. M. Kalvius, A. Martin, M. K. Krause, I. Halevy, J. Gal, W. Schafer, G. Will, M. Hillberg, and R. Wappling, Phys. Rev. B **53**, 9143 (1996).
[11] K. Kamazawa, Y. Tsunoda, H. Kadowaki, and K. Kohn, Phys. Rev. B **68**, 024412 (2003).
[12] T. Watanabe, S. Takita, K. Tomiyasu, and K. Kamazawa, Phys. Rev. B **92**, 174420 (2015).
[13] T. Nitta, Z. Terada, and S. Hayakawa, J. Am. Ceram. Soc. **63**, 295 (1980).
[14] J. Ding, T. J. Mc. Avoy, R. E. Cavicchi, and S. Semancik, Sens. Actuators B **77**, 597 (2001).
[15] K. Mukherjee and S. B. Majumder, J. Appl. Phys. **106**, 064912 (2009).
[16] Y. Hou, X. Li, Q. Zhao, X. Quan, and G. Chen, Adv. Funct. Mater. **20**, 2165 (2010).
[17] J. A. Toledo-Antonio, N. Nava, M. Martınez, and X. Bokhimi, Appl. Catal. A **234**, 137 (2002).

[18] M. Kobayashi, H. Shirai, and M. Nunokawa, Indust. Eng. Chem. Res. **41**, 2903 (2002).
[19] G. Maggioni, A. Vomiero, S. Carturan, C. Scian, G. Mattei, M. Bazzan, C. J. Fernandez, P. Mazzoldi, A. Quaranta, and G. D. Mea, Appl. Phys. Lett. **85**, 5712 (2004).
[20] K. A. Bogle, S. D. Dhole, and V. N. Bhoraskar, Nanotechnology **17**, 3204 (2006).
[21] P. Gangopadhyay, R. Kesavamoorthy, S. Bera, P. Magudapathy, K. G. M. Nair, B. K. Panigrahi, and S. V. Narasimhan, Phys. Rev. Lett. **94**, 047403 (2005).
[22] C. Yao, Q. Zeng, G. F. Goya, T. Torres, J. Liu, H. Wu, M. Ge, Y. Zeng, Y. Wang, and J. Z. Jiang, J. Phys. Chem. C **111**, 12274 (2007).
[23] T. Sato, K. Haneda, M. Seki, and T. Iijima, Appl. Phys. A **50**, 13 (1990).
[24] P. Puspitasari, U. A. Rizkiaa, S. Sukarnia, A. A. Permanasari, A. Taufiq, and A. B. N. R. Putra, Mater. Res. **24**, e20200300 (2021).
[25] C. N. Chinnasamy, A. Narayanasamy, N. Ponpandian, and K. Chattopadhyay, Mater. Sci. Eng. A **304**, 983 (2001).
[26] S. B. Singh, Ch. Srinivas, B. V. Tirupanyam, C. L. Prajapat, M. R. Singh, S. S. Meena, P. Bhatt, S. M. Yusuf, and D. L. Sastry, Ceram. Int. **42**, 19179 (2016).
[27] H. M. Zaki, S. H. Al-Heniti, and T. A. Elmosalami, J. Alloys Compd. **633**, 104 (2015).
[28] S. K. Jena, D. C. Joshi, Z. Yan, Y. Qi, S. Ghosh, and S. Thota, J. Appl. Phys. **128**, 073908 (2020).
[29] R. Zhang, Q. Yuan, R. Ma, X. Liu, C. Gao, M. Liu, C. Jiaac, and H. Wang, RSC Adv. **7**, 21926 (2017).
[30] J. S. Gardner, B. D. Gaulin, S.-H. Lee, C. Broholm, N. P. Raju, and J. E. Greedan, Phys. Rev. Lett. **83**, 211 (1999).
[31] A. Keren and J. S. Gardner, Phys. Rev. Lett. **87**, 177201 (2001).
[32] S. Thota, M. Reehuis, A. Maljuk, A. Hoser, J.-U. Hoffmann, B. Weise, A. Waske, M. Krautz, D. C. Joshi, S. Nayak, S. Ghosh, P. Suresh, K. Dasari, S. Wurmehl, O. Prokhnenko, and B. Büchner, Phys. Rev. B **96**, 144104 (2017).
[33] S. Nayak, K. Dasari, D. C. Joshi, P. Pramanik, R. Palai, A. Waske, R. N. Chauhan, N. Tiwari, T. Sarkar, and S. Thota, J. Appl. Phys. **120**, 163905 (2016).
[34] S. Akhter, M. A. Hakim, S. M. Hoque, R. Mathieu, and P. Nordblad, J. Magn. Magn. Mater. **452**, 261 (2018).
[35] S. Akhter, M. A. Hakim, S. M. Hoque, and H. N. Das, Solid State Commun. **326**, 114181 (2021).
[36] F. H. Bo, Y. S. Yan, Z. P. Feng, W. H. Yuan, L. X. Lin, J. C. Mei, Z. Q. Sheng, C. Y. Hai, and W. Z. Guo, Chin. Phys. Lett. **24**, 2108 (2007).
[37] P. Tehranian, A. Shokuhfar, and H. Bakhshi, J. Supercond. Nov. Magn. **32**, 1013 (2019).
[38] Q. Yuan, L. L. Pan, R. Liu, J. M. Wang, Z. Z. Liao, L. L. Qin, J. Bi, D. J. Gao, and J. T. Wu, J. Electron. Mater. **47**, 3608 (2018).
[39] X. Zhu, C. Cao, S. Su, A. Xia, H. Zhang, H. Li, Z. Liu, and C. Jin, Ceram. Int. **47**, 15173 (2021).
[40] J. G. Jolley, G. G. Geesey, M. R. Hankins, R. B. Wright, and P. L. Wichlacz, Appl. Surf. Sci. **37**, 469 (1989).
[41] L. Wu, H. Wu, H. Zhang, H. Cao, G. Hou, Y. Tang, and G. Zheng, Chem. Eng. J. **334**, 1808 (2018).
[42] T. Yamashita and P. Hayes, Appl. Surf. Sci. **254**, 2441 (2008).
[43] See Supplemental Material at http://link.aps.org/supplemental/10.1103/PhysRevB.106.174402 for details of Mossbauer spectroscopic studies on confirmation of Fe^{3+} state in the sample.
[44] S. Nayak, S. Thota, D. C. Joshi, M. Krautz, A. Waske, A. Behler, J. Eckert, T. Sarkar, M. S. Andersson, R. Mathieu, V. Narang, and M. S. Seehra, Phys. Rev. B **92**, 214434 (2015).
[45] J. G. Kim, D. L. Pugmire, D. Bhattagila, and M. A. Langell, Appl. Surf. Sci. **165**, 70 (2000).
[46] R. N. Bhowmik, R. Ranganathan, and R. Nagarajan, J. Magn. Magn. Mater. **299**, 327 (2006).
[47] A. Malinowski, V. L. Bezusyy, R. Minikayev, P. Dziawa, Y. Syryanyy, and M. Sawicki, Phys. Rev. B **84**, 024409 (2011).
[48] R. Kumar, P. Yanda, and A. Sundaresan, Phys. Rev. B **103**, 214427 (2021).
[49] P. Bag, P. R. Baral, and R. Nath, Phys. Rev. B **98**, 144436 (2018).
[50] K. de Strooper, Phys. Status Solidi A **39**, 431 (1977).
[51] S. Thota, V. Narang, S. Nayak, S. Sambasivam, B. C. Choi, T. Sarkar, M. S. Andersson, R. Mathieu, and M. S. Seehra, J. Phys.: Condens. Matter **27**, 166001 (2015).
[52] B. Musicó, Q. Wright, T. Z. Ward, A. Grutter, E. Arenholz, D. Gilbert, D. Mandrus, and V. Keppens, Phys. Rev. Mater. **3**, 104416 (2019).